Nano Research 2013, 6(7): 478–484
DOI 10.1007/s12274-013-0325-7
Research Article

ISSN 1998-0124
CN 11-5974/O4

Solution-processable graphene mesh transparent electrodes for organic solar cells

Qian Zhang[1], Xiangjian Wan[1], Fei Xing[2], Lu Huang[1], Guankui Long[1], Ningbo Yi[1], Wang Ni[1], Zhibo Liu[2], Jianguo Tian[2], and Yongsheng Chen[1] (✉)

[1] *Key Laboratory for Functional Polymer Materials and Centre for Nanoscale Science and Technology, Institute of Polymer Chemistry, College of Chemistry, Nankai University, Tianjin 300071, China*

[2] *The Key Laboratory of Weak Light Nonlinear Photonics, Ministry of Education, Teda Applied Physics School and School of Physics, Nankai University, Tianjin 300071, China*

Received: 19 March 2013
Revised: 18 April 2013
Accepted: 18 April 2013

KEYWORDS

graphene,
transparent electrode,
photolithography,
mesh electrode,
organic photovoltaic cells

ABSTRACT

Graphene mesh electrodes (GMEs) with good conductivity and transparency have been fabricated by the standard industrial photolithography and O_2 plasma etching process using graphene solutions. Organic photovoltaic (OPV) cells using GMEs as the transparent electrodes with a blend of poly-(3-hexylthiophene)/phenyl-C_{61}-butyric acid methyl ester (P3HT/PC_{61}BM) as the active layer have been fabricated and exhibit a power conversion efficiency (PCE) of 2.04%, the highest PCE for solution-processed graphene transparent electrode-based solar cells reported to date.

Organic photovoltaic (OPV) cells have drawn more and more attention as a non-exhaustible and clean energy source with the advantages of low-cost, light-weight, large-area, and high mechanical flexibility [1]. Transparent electrode materials are the critical component of OPV cells. Currently, indium tin oxide (ITO) has been the dominant material used as the electrodes because it offers high transparency in the visible range of the solar spectrum as well as good conductivity. However, it appears to be increasingly problematic to continue to rely on ITO transparent electrodes due to the scarcity of indium reserves, the intensive processing requirements, its instability in acid or base, and the highly brittle nature of the metal oxide [2, 3]. Seeking replacement materials for ITO with comparable performance and lower cost is in high demand.

In recent years, graphene, a two-dimensional carbon material, has attracted great attention owing

Address correspondence to yschen99@nankai.edu.cn

to its intrinsic outstanding electronic [4, 5], optical [6], thermal [7] and mechanical [8] properties. Graphene-based materials have been widely studied as transparent electrodes [9–33]. Among the general methods to obtain graphene thin films such as micromechanical exfoliation, epitaxial growth, chemical vapor deposition (CVD) and reduced graphene oxide (rGO), the last method demonstrates the advantages of low cost, simplicity of fabrication technique, and ease of scale-up for practical applications. However, there is an unavoidable tradeoff between the transparency and conductivity for rGO-based transparent electrodes. OPV cells based on rGO electrodes generally exhibit poor power conversion efficiencies (PCE) of less than 1.0% [15–20], mainly owing to their combined characteristics of large sheet resistance and low transparency when used in OPV cells. So the key issue for graphene-based transparent electrodes is to obtain films with both good conductivity and appropriate transparency.

Meanwhile, metal grid electrodes with high transparency have been widely investigated and comparable OPV performances with ITO have also been obtained [34–37]. However, discontinuities in the conductivity of these films on a local scale are generated in the active layer and recombine before diffusing to the closest grid line. In addition, most methods for the fabrication of such patterned metal grids are cumbersome and involve costly patterning techniques.

Inspired by such metal grid or mesh electrodes, graphene mesh electrodes (GME) have been prepared in this study. In previous work, Zhang et al. reported the fabrication of graphene nanomesh (GNM) using anodic aluminum oxide (AAO) as an etch mask with poly(methyl methacrylate) as the adhesion layer between the AAO template and the rGO sheets assembled on a Si/SiO_2 substrate together with O_2 plasma etching [38], and Mullen patterned graphene using evaporated Al as the mask and O_2 plasma to remove graphene not protected by the mask [22]. In this work, we report the fabrication of GMEs by using the standard industrial photolithography and O_2 plasma etching process, which is a conventional technology in the semiconductor industry and is practical for producing graphene mesh transparent electrodes on a large scale. OPV devices employing the GMEs as the transparent electrodes with poly-(3-hexylthiophene)/phenyl-C_{61}-butyric acid methyl ester (P3HT/$PC_{61}BM$) as the active layer [1] have been fabricated and exhibit a PCE of 2.04%, which corresponds to 67% of the efficiency of the control device using ITO as the transparent electrode. To the best of our knowledge, this is the highest PCE for a solution-processed graphene transparent electrode-based OPV cell.

The fabrication of GMEs by the conventional photolithography and O_2 plasma etching methods is illustrated in Fig. 1. First, a GO dispersion in water was spin-coated on a pre-cleaned quartz substrate and was then thermally annealed at 950 °C to restore graphene film conductivity. GO was prepared with a modified Hummers' method as described in our previous work [39]. The thickness of the as prepared

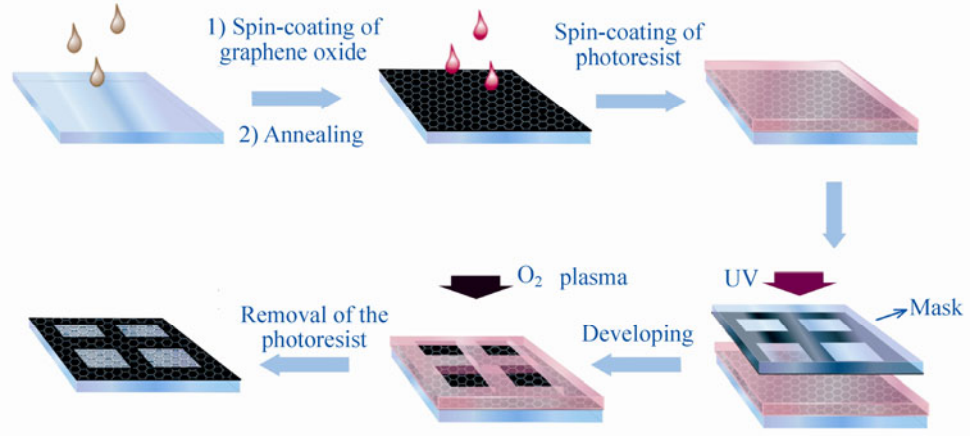

Figure 1 Illustration of the schematic steps for the preparation of the graphene mesh electrodes.

rGO film is ~100 nm. Afterwards, the photolithography and O_2 plasma etching process were conducted. The standard industrial photolithography process was followed, which includes the spin-coating of positive photoresist on the surface of the rGO film, exposure to ultraviolet light, development, O_2 plasma etching steps, and the removal of the photoresist patterns. Details are given in the Electronic Supplementary Materials (ESM). The graphene grid patterns were obtained by the protection of the photoresist patterns, and the unprotected graphene sheets were etched away by O_2 plasma. In this way, the pattern of the resulting GME structures can be controlled precisely and follows exactly that of the mask used (Figs. 2(a) and 2(b)). Atomic force microscopy (AFM) images are shown in the ESM (Figs. S1(a) and S1(b)). The mask used had a 50 μm period and 10 μm line width and can be conveniently adjusted. The theoretical transparency of the mask is 70%, which is determined by the line width of the grid lines, or equivalently, the opening ratio of the grid. The transparency of the graphene electrode before the mask-based etching is ~8% and the transparency of the electrode after the mask-based etching has been greatly improved to 65%, slightly smaller than the mask's theoretical value of 70% (Fig. 2(c)). This is probably due to the unavoidable edge effect of the mask during the etching process. It should be noted that the patterned graphene films prepared following the above procedure offer the promise of application not only for transparent electrodes but also for integrated circuits and other devices.

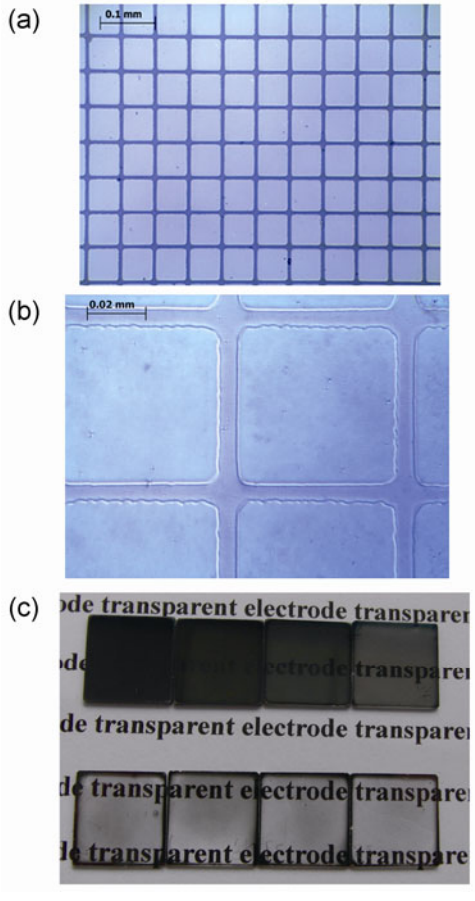

Figure 2 (a) and (b) Microscopy images of the GME with a 50 μm period and 10 μm line width. The scale bar in the microscopy images is 0.1 mm (a) and 0.02 mm (b). (c) Optical images of the as-prepared rGO films (the upper image) and the GMEs (the lower image).

Before the etching, the film with 8% transmittance at 550 nm had a sheet resistance of about 150 Ω·sq.$^{-1}$. The depth of the pits is mainly dependent on the O_2 plasma etching time, which also impacts the transparency. With the increase of the the O_2 plasma etching time (from 4 to 10 min), the depth of the pits increased (see Fig. 3), and the transparency also improved significantly over the whole spectral region, as shown in Fig. 4. Other masks with different patterning periods and line widths have also been used to prepare the GMEs, such as one with a 50 μm period and 20 μm line width and another one with a 30 μm period and 10 μm line width. However, the maximum transparencies obtained were 50% and 56% respectively for these two cases. Overall, the GME with 50 μm period and 10 μm line width, which has a higher transparency and comparable sheet resistance, gave the best performance as the transparent electrode in OPV.

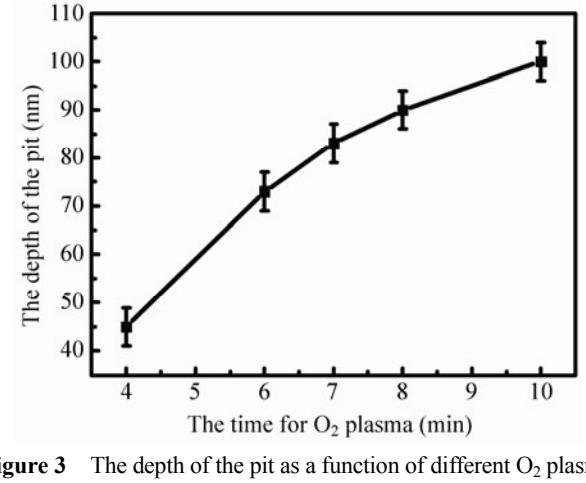

Figure 3 The depth of the pit as a function of different O_2 plasma etching times.

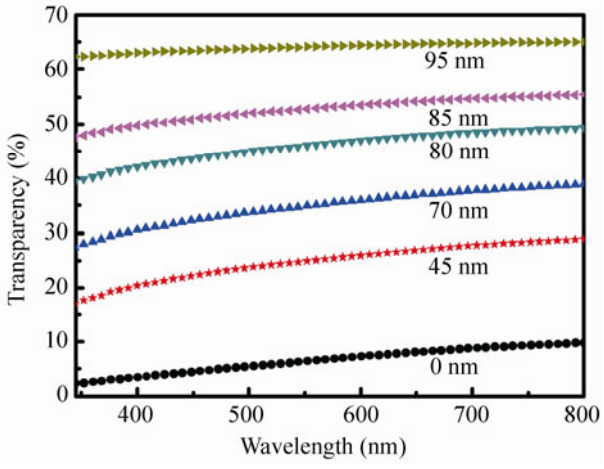

Figure 4 Optical transmittance spectra of GMEs with different depths of the pits.

As expected, the conductivity of the as-prepared GMEs based on the same mask is also closely related to the depth of the pits. With a given initial film thickness of ~100 nm, a concomitant decrease in film conductivity was observed with an increase of the depth of the pit from 40 to 100 nm, controlled by O_2 plasma etching time (Fig. 5). Under our conditions, the etched graphene films could reach a sheet resistance of 700 Ω·sq.$^{-1}$ (transmittance of 65% at 550 nm), which is much lower than the resistance of 17.9 kΩ·sq.$^{-1}$ (transmittance of 69% at 550 nm) without etching [15].

To investigate the suitability of the GMEs as anodes in OPV cells, devices with the structure of GME/PEDOT:PSS/P3HT:PC_{61}BM/LiF/Al (PEDOT:PSS = poly(3,4-ethylenedioxythiophene): poly(styrenesulfonate) were fabricated (Fig. 6; details of the fabrication of the device are in the ESM). Normally, the rGO film surface is hydrophobic, which makes it difficult to get a uniform PEDOT:PSS layer. However, our as-obtained GMEs are more hydrophilic than those not etched, because the O_2 plasma can produce some oxygen-containing functional groups on the surface. The characteristic parameters of OPV devices using GMEs with different transparency and sheet resistance together, with the reference device using ITO as the transparent electrodes, are listed in Table 1. The open circuit voltage (V_{oc}) of the devices based on GMEs is about 0.52 V, which is comparable with that of ITO-based devices. Meanwhile, on going from device 1 to device 4 when the graphene is not completely etched away for the etched areas, the short-circuit current density (J_{sc}) increases from 2.97 to 6.35 mA·cm^{-2} as the thickness of the graphene in the etched areas is

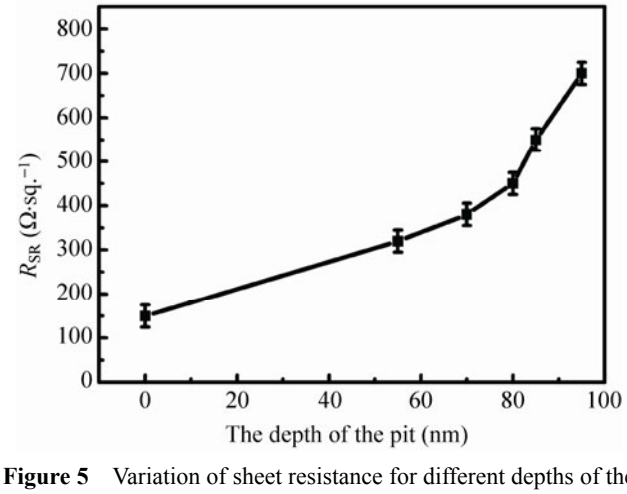

Figure 5 Variation of sheet resistance for different depths of the pits in the GMEs.

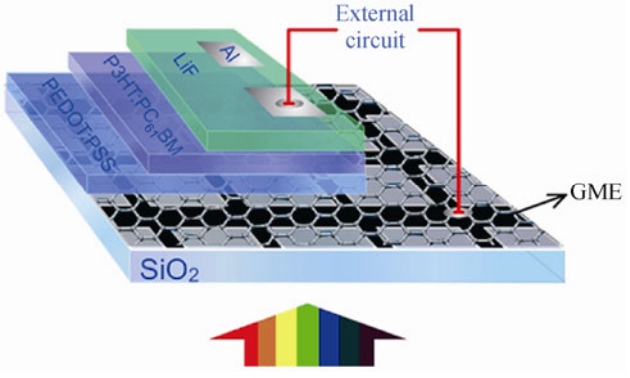

Figure 6 Configuration of the OPV device GME/PEDOT:PSS/P3HT:PC_{61}BM/LiF/Al.

Table 1 Summary of the photovoltaic performance of OPV devices based on GMEs with different depths of the pits (d), transparency (T) and sheet resistance (R_{SR}) and the reference device based on ITO

Device (d, T, R_{SR} of GME)	V_{oc} (V)	J_{sc} (mA·cm^{-2})	FF	PCE (%)
1 (40–45 nm, 21%, 401 Ω·sq.$^{-1}$)	0.50	2.97	0.57	0.86
2 (70–75 nm, 38%, 486 Ω·sq.$^{-1}$)	0.52	3.50	0.54	0.99
3 (80–85 nm, 46%, 512 Ω·sq.$^{-1}$)	0.54	5.66	0.55	1.66
4 (85–90 nm, 55%, 608 Ω·sq.$^{-1}$)	0.54	6.35	0.58	2.04
5 (~100 nm, 65%, 750 Ω·sq.$^{-1}$)	0.52	2.39	0.34	0.41
ITO	0.56	8.98	0.60	3.00

reduced, and thus the enhancement in transparency directly results in a great improvement in the PCE from 0.86% to 2.04%. However after the transparency reaches ~65%, J_{sc} and FF are markedly reduced, as in the case for device 5 in Table 1. The Raman spectrum of the GME of device 5 (Fig. 7) recorded for the patterned regions of the graphene mesh on quartz substrates shows that the unetched channels display the characteristic graphene D and G bands at 1,354 and 1,596 cm^{-1}. However, for the etched area of GME, both the D and G bands disappear, indicating that no residual graphene material remains in the pit area under these conditions. We thus believe that the graphene in the pit area was totally etched away under this condition, which resulted in discontinuities of charge transportation channels on a local scale comparable to the spacing of the grids, and this would significantly reduce the efficiency of the charge collection. Similar results have been observed for metal mesh electrodes [34–36]. We also investigated the photovoltaic performance of cells based on GMEs with different initial thickness when the graphene in the pits is completely etched away. The photovoltaic characteristic results are listed in Table S1 (in the ESM): the values of J_{sc} and FF are very low, as discussed above for the case of device 5. Therefore, there is an optimum depth of the pits for the GMEs in order to achieve the best OPV performance.

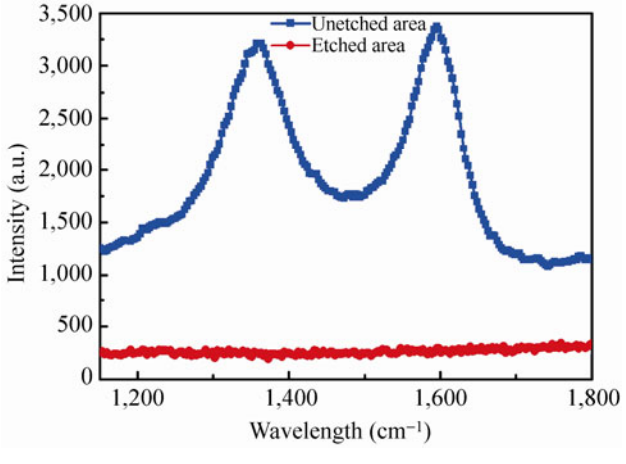

Figure 7 The Raman spectra for the GME with 65% transparency for device 5 in Table 1. The unetched area exhibits the characteristic D and G peaks of graphene materials. For the etched area, the absence of the typical D and G peaks indicates the complete removal of the graphene in the etched area.

For comparison, the control device using ITO as the electrode has been tested under the same conditions and a PCE of 3.00% was obtained with a V_{oc} of 0.56 V, J_{sc} of 8.98 $mA{\cdot}cm^{-2}$ and a FF of 0.60 (Fig. 8). While the overall performance of devices using GME is still lower than that using ITO, it is better than that of analogous cells based on rGO reported previously [15–20]. The lower efficiency of the device based on GMEs is probably still mainly due to the low transparency. The devices prepared in this study also showed much higher FF (0.58) than the previously reported graphene film electrode devices (0.48) [15–20], which is due to the well-established heterojunction and the low series resistance of the device configuration. Another possible reason is that the shunt resistance (R_{sh}) of the GME-based OPV device gave a value of 1.52×10^3 $\Omega{\cdot}cm^{-2}$, which is slightly higher than that of the ITO-based OPV device (1.42×10^3 $\Omega{\cdot}cm^{-2}$). The shunt resistance (R_{sh}) is given by the inverse gradient of the *J–V* curves at the open-circuit voltage. Also, we noted that the device based on GME exhibited good diode behavior with a rectification ratio of approximately three orders of magnitude at biases ±1 V (Fig. S2 in the ESM). All these factors contributed to the improved performance of the GME-based OPV devices. Further studies are in progress to improve the performance of the GME-based solar cell devices by optimizing the transparency of the GMEs and controlling the interfacial contact between the graphene electrode and the PEDOT:PSS layer.

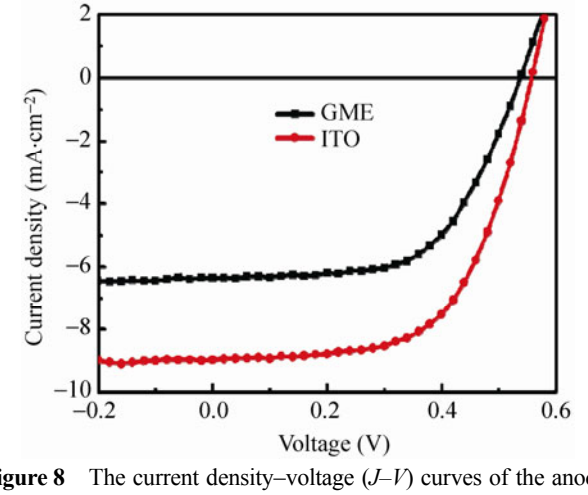

Figure 8 The current density–voltage (*J–V*) curves of the anode/PEDOT:PSS/P3HT:PC_{61}BM/LiF/Al photovoltaic cells with ITO (red) or GME (black) as the anode under illumination of AM.1.5, 100 $mW{\cdot}cm^{-2}$.

In conclusion, OPV devices based on GMEs have been fabricated for the first time and 2.04% PCE has been achieved, the highest PCE value obtained to date using solution-processed graphene materials as the transparent electrode material. Using the standard industrial photolithography technique, the mesh electrode patterns can be controlled precisely to achieve a balance of the conductivity and transparency. These results, combined with the solution-processable and readily available GO, make the application of graphene as the transparent electrode in OPV and other optoelectronic devices a realistic proposition.

Acknowledgements

The authors gratefully acknowledge the financial support from the Ministry of Science and Technology of the People's Republic of China (Grants Nos. 2012CB933401 and 2011DFB50300), the National Natural Science Foundation of China (Grants Nos. 51273093 and 50933003) and Natural Science Foundation of Tianjin (Grant No. 10ZCGHHZ00600).

Electronic Supplementary Material: Supplementary material (experimental details, AFM images of GME, plots of logarithmic current density vs. voltage of OPV cells based on GME) is available in the online version of this article at http://dx.doi.org/10.1007/s12274-013-0325-7.

References

[1] Li, G.; Shrotriya, V.; Huang, J. S.; Yao, Y.; Moriarty, T.; Emery, K.; Yang, Y. High-efficiency solution processable polymer photovoltaic cells by self-organization of polymer blends. *Nat. Mater*. **2005**, *4*, 864–868.

[2] Boehme, M.; Charton, C. Properties of ITO on PET film in dependence on the coating conditions and thermal processing. *Surf. Coat. Technol*. **2005**, *200*, 932–935.

[3] Andersson, A.; Johansson, N.; Broms, P.; Yu, N.; Lupo, D.; Salaneck, W. R. Fluorine tin oxide as an alternative to indium tin oxide in polymer LEDs. *Adv. Mater*. **1998**, *10*, 859–863.

[4] Novoselov, K. S.; Geim, A. K.; Morozov, S. V.; Jiang, D.; Zhang, Y.; Dubonos, S. V.; Grigorieva, I. V.; Firsov, A. A. Electric field effect in atomically thin carbon films. *Science* **2004**, *306*, 666–669.

[5] Avouris, P.; Chen, Z.; Perebeinos, V. Carbon-based electronics. *Nat. Nanotechnol*. **2007**, *2*, 605–615.

[6] Geim, A. Graphene: Status and prospects. *Science* **2009**, *324,* 1530–1534.

[7] Sui, D.; Huang, Y.; Huang, L.; Liang, J.; Ma, Y.; Chen, Y. Flexible and transparent electrothermal film heaters based on graphene materials. *Small* **2011**, *7*, 3186–3192.

[8] Liang, J.; Huang, Y.; Zhang, L.; Wang, Y.; Ma, Y.; Guo, T.; Chen, Y. Molecular-level dispersion of graphene into poly(vinyl alcohol) and effective reinforcement of their nanocomposites. *Adv. Funct. Mater*. **2009**, *19*, 2297–2302.

[9] Eda, G.; Fanchini, G.; Chhowalla, M. Large-area ultrathin films of reduced graphene oxide as a transparent and flexible electronic material. *Nat. Nanotechnol*. **2008**, *3*, 270–274.

[10] Wan, X.; Huang, Y.; Chen, Y. Focusing on energy and optoelectronic applications: A journey for graphene and graphene oxide at large scale. *Acc. Chem. Res*. **2012**, *45*, 598–607.

[11] Wan, X.; Long, G.; Huang, L.; Chen, Y. Graphene—A promising material for organic photovoltaic cells. *Adv. Mater*. **2011**, *23*, 5342–5358.

[12] Huang, X.; Zeng, Z.; Fan, Z.; Liu, J.; Zhang, H. Graphene-based electrodes. *Adv. Mater*. **2012**, *24*, 5979–6004.

[13] He, Q.; Wu, S.; Yin, Z.; Zhang, H. Graphene-based electronic sensors. *Chem. Sci*. **2012**, *3*, 1764–1772.

[14] Huang, X.; Qi, X.; Boeyab, F.; Zhang, H. Graphene-based composites. *Chem. Soc. Rev*. **2012**, *41*, 666–686.

[15] Xu, Y.; Long, G.; Huang, L.; Huang, Y.; Wan, X.; Ma, Y.; Chen, Y. Polymer photovoltaic devices with transparent graphene electrodes produced by spin-casting. *Carbon* **2010**, *48*, 3308–3311.

[16] Wu, J.; Becerril, H. A.; Bao, Z.; Liu, Z.; Chen, Y.; Peumans, P. Organic solar cells with solution-processed graphene transparent electrodes. *Appl. Phys. Lett*. **2008**, *92*, 263302.

[17] Eda, G.; Lin, Y. Y.; Miller, S.; Chen, C. W.; Su, W. F.; Chhowalla, M. Transparent and conducting electrodes for organic electronics from reduced graphene oxide. *Appl. Phys. Lett*. **2008**, *92*, 233305

[18] Tung, V. C.; Chen, L. M.; Allen, M. J.; Wassei, J. K.; Nelson, K.; Kaner, R. B.; Yang, Y. Low-temperature solution processing of graphene–carbon nanotube hybrid materials for high-performance transparent conductors. *Nano Lett*. **2009**, *9*, 1949–1955.

[19] Yin, Z.; Sun, S.; Salim, T.; Wu, S.; Huang, X.; He, Q.; Lam, Y. M.; Zhang, H. Organic photovoltaic devices using highly flexible reduced graphene oxide films as transparent electrodes. *ACS Nano* **2010**, *4*, 5263–5268.

[20] Geng, J.; Liu, L.; Yang, S. B.; Youn, S. C.; Kim, D. W.; Lee, J. S.; Choi, J. K.; Jung, H. T. A simple approach for

preparing transparent conductive graphene films using the controlled chemical reduction of exfoliated graphene oxide in an aqueous suspension. *J. Phys. Chem. C* **2010**, *114*, 14433–14440.

[21] Pang, S.; Tsao, H. N.; Feng, X.; Müellen, K. Patterned graphene electrodes from solution-processed graphite oxide films for organic field-effect transistors. *Adv. Mater*. **2009**, *21*, 3488–3491.

[22] Wang, X.; Zhi, L.; Müllen, K. Transparent, conductive graphene electrodes for dye-sensitized solar cells. *Nano Lett*. **2008**, *8*, 323–327.

[23] Wu, J.; Agrawal, M.; Becerril, H. A.; Bao, Z.; Liu, Z.; Chen, Y.; Peumans, P. Organic light-emitting diodes on solution-processed graphene transparent electrodes. *ACS Nano* **2010**, *4*, 43–48.

[24] De Arco, L. G.; Zhang, Y.; Schlenker, C. W.; Ryu, K.; Thompson, M. E.; Zhou, C. Continuous, highly flexible, and transparent graphene dilms by chemical vapor deposition for organic photovoltaics. *ACS Nano* **2010**, *4*, 2865–2873.

[25] Choe, M.; Lee, B. H.; Jo, G.; Park, J.; Park, W.; Lee, S.; Hong, W. K.; Seong, M. J.; Kahng, Y. H.; Lee, K.; et al. Efficient bulk-heterojunction photovoltaic cells with transparent multi-layer graphene electrodes. *Org. Electron*. **2010**, *11*, 1864–1869.

[26] Choi, Y. Y.; Kang, S. J.; Kim, H. K.; Choi, W. M.; Na, S. I. Multilayer graphene films as transparent electrodes for organic photovoltaic devices. *Sol. Energ. Mat. Sol. C* **2012**, *96*, 281–285.

[27] Wang, Y.; Chen, X.; Zhong, Y.; Zhu, F.; Loh, K. P. Large area, continuous, few-layered graphene as anodes in organic photovoltaic devices. *Appl. Phys. Lett*. **2009**, *95*, 063302.

[28] Wang, Y.; Tong, S. W.; Xu, X. F.; Öezyilmaz, B.; Loh, K. P. Interface engineering of layer-by-layer stacked graphene anodes for high-performance organic solar cells. *Adv. Mater*. **2011**, *23*, 1514–1518.

[29] Kim, K. S.; Zhao, Y.; Jang, H.; Lee, S. Y.; Kim, J. M.; Kim, K. S.; Ahn, J. H.; Kim, P.; Choi, J. Y.; Hong, B. H. Large-scale pattern growth of graphene films for stretchable transparent electrodes. *Nature* **2009**, *457*, 706–710.

[30] Zhu, Y.; Sun, Z.; Yan, Z.; Jin, Z.; Tour, J. M. Rational design of hybrid graphene films for high-performance transparent electrodes. *ACS Nano* **2011**, *5*, 6472–6479.

[31] Lin, P.; Choy, W. H.; Zhang, D.; Xie, F.; Xin, J.; Leung, C. W. Semitransparent organic solar cells with hybrid monolayer graphene/metal grid as top electrodes. *Appl. Phys. Lett*. **2013**, *102*, 113303.

[32] Liu, J.; Yin, Z.; Cao, X.; Zhao, F.; Wang, L.; Huang, W.; Zhang, H. Fabrication of flexible, all-reduced graphene oxide non-volatile memory devices. *Adv. Mater*. **2013**, *25*, 233–238.

[33] Liu, J.; Lin, Z.; Liu, T.; Yin, Z.; Zhou, X.; Chen, S.; Xie, L.; Boey, F.; Zhang, H.; Huang, W. Multilayer stacked low-temperature-reduced graphene oxide films: Preparation, characterization, and application in polymer memory devices. *Small* **2010**, *6*, 1536–1542.

[34] Kang, M. G.; Kim, M. S.; Kim, J.; Guo, L. Organic solar cells using nanoimprinted transparent metal electrodes. *Adv. Mater*. **2008**, *20*, 4408–4413.

[35] Lee, J. Y.; Connor, S. T.; Cui, Y.; Peumans, P. Solution-processed metal nanowire mesh transparent electrodes. *Nano Lett*. **2008**, *8*, 689–692.

[36] Hecht, D. S.; Hu, L.; Irvin, G. Emerging transparent electrodes based on thin films of carbon nanotubes, graphene, and metallic nanostructures. *Adv. Mater*. **2011**, *23*, 1482–1513.

[37] Yang, L.; Zhang, T.; Zhou, H.; Price, S. C.; Wiley, B. J.; You, W. Solution-processed flexible polymer solar cells with silver nanowire electrodes. *ACS Appl. Mater. Interfaces* **2011**, *3*, 4075–4084.

[38] Zeng, Z.; Huang, X.; Yin, Z.; Li, H.; Chen, Y.; Li, H.; Zhang, Q.; Ma, J.; Boey, F.; Zhang, H. Fabrication of graphene nanomesh by using an anodic aluminum oxide membrane as a template. *Adv. Mater.* **2012**, *24*, 4138–4142.

[39] Zhang, L.; Liang, J.; Huang, Y.; Ma, Y.; Wang, Y.; Chen, Y. Size-controlled synthesis of graphene oxide sheets on a large scale using chemical exfoliation. *Carbon* **2009**, *47*, 3365–3368.